Published in final edited form as:
Proteins. 2010 December ; 78(16): 3458–3472. doi:10.1002/prot.22832.

Beta-barrel models of soluble amyloid beta oligomers and annular protofibrils

Yinon Shafrir[1], **Stewart R. Durell**[1], **Andriy Anishkin**[2], and **H. Robert Guy**[1]

[1]Laboratory of Cell Biology, CCR, NCI, National Institutes of Health, Bldg. 37 Rm 2108, Bethesda, MD 20892-4258

[2]Department of Biology, University of Maryland, College Park, Maryland 20742 U.S.A.

Abstract

Both soluble and membrane-bound pre-fibrillar assemblies of Abeta (Aβ) peptides have been associated with Alzheimer's disease (AD). The size and nature of theses assemblies vary greatly and are affected by many factors. Here we present models of soluble hexameric assemblies of Aβ42 and suggest how they can lead to larger assemblies and eventually to fibrils. The common element in most of these assemblies is a six-stranded β-barrel formed by the last third of Aβ42, which is composed of hydrophobic residues and glycines. The hydrophobic core β-barrels of the hexameric models are shielded from water by the N-terminus and central segments. These more hydrophilic segments were modeled to have either predominantly β or predominantly α secondary structure. Molecular dynamics simulations were performed to analyze stabilities of the models. The hexameric models were used as starting points from which larger soluble assemblies of 12 and 36 subunits were modeled. These models were developed to be consistent with numerous experimental results.

Keywords

Abeta; molecular models; structure prediction; Alzheimer's disease; protein structure; molecular dynamics; molecular assemblies

INTRODUCTION

Amyloid beta (Aβ) peptides play a pivotal role in the development of Alzheimer's disease (AD)[4]. Formally it was thought that the fibrils were the primary cause of AD[17]; however, recent studies indicate that pre-fibrillar oligomeric assemblies are more toxic than fibrils[47] and that interactions of oligomers with membranes may be involved[1, 46]. Both experimental and theoretical studies of Aβ assemblies are complicated by heterogeneity, the dynamic nature of many oligomers, and the possibility that isolation methods alter the assemblies. Aβ preparations in solution typically have numerous types of pre-fibrillar assemblies composed of differing numbers of subunits, which have differing degrees of structural order, and all this changes with time. Names of these assemblies include low-order oligomers[44, 48, 52], Aβ-derived diffusible ligands (ADDLs)[15, 32], paranuclei[5], globulomers[2], Aβ*56[35], β-amyballs[53], amylospheroids[21], annular protofibrils[26, 33, 34], and protofibrils[19, 20, 51].

*Corresponding author: permanent address H. Robert Guy 6510 Tahawash St. Cochiti Lake, NM 87083 Telephone: 505-465-2445 or 301-767-5455 (cell) Fax: 301-402-4724 bg4y@nih.gov.
Yinon Shafrir: yinon@nih.gov
Stewart Durell: Stewart_Durell@nih.gov
Andriy Anishkin: anishkin@icqmail.com

Here we present structural models of soluble assemblies, beginning with hexamers, and then building up to dodecamers and annular protofibrils. In explaining our models, and the rationale for developing them, we use a nomenclature in which Aβ42 is divided into three segments of equal length, which we call S1, S2, and S3 (Fig. 1A). This division illustrates the amphiphilic nature of the peptide; S1 is composed primarily of hydrophilic residues, S2 has five consecutive hydrophobic residues (17–21) flanked by more hydrophilic segments, and S3 is composed entirely of hydrophobic and apolar glycine residues. In NMR-based models of monomers, oligomers, and fibrils[40, 41, 50, 55], and in our models, the hydrophilic S1 segment is the least ordered and most ambiguous segment. In contrast, the hydrophobic S3 segment is the most ordered and least ambiguous; it is modeled to form a six-stranded β-barrel in the core of hexamers.

MATERAL AND METHODS

Four categories of criteria used in developing our models are explained below.

Experimental constraints

Aβ monomers and some low-order soluble oligomers appear to be relatively disordered[22], and we have not attempted to model these types of structures. However, recent studies indicate that even relatively small Aβ may possess a substantial amount of ordered structure. Hydrogen/deuterium exchange rate (or amide protection) studies of Aβ oligomers indicate that most backbone hydrogens of the hydrophobic S3 segment are inaccessible to solvent[9, 27, 28, 54–56], suggesting that S3 is relatively buried and has an ordered structure with rather complete backbone H bonding. We have modeled this region to form a hydrophobic core in which all polar backbone atoms of the central portion of these segments form hydrogen bonds.

A recent study of large Aβ42 oligomers (40–170 kDa or 8–38 peptides) using attenuated total reflection-FTIR spectroscopy found 48–57% of their secondary structure to be antiparallel β-sheets, while ~20–26% was random coil and/or helical[9]. Prior to this study we had developed both parallel and antiparallel β-barrel models of Aβ oligomers. These results are a major reason why we now favor the antiparallel models. The helical content was higher (33%) in oligomers incubated for less than one hour; consistent with earlier proposals that some helical structure precedes formation of β-sheets[29, 30]. We have included possible transition models in which the latter part of the S1 segment and most of the S2 segment is helical.

Aβ preglobulomers (2–6 subunits) and globulomers (12–16 subunits) formed in the presence of negatively charged detergent (SDS) or fatty acids are also primarily β. Solution NMR studies of preglobulomers support models for dimeric components of these assemblies in which residues 18–22 and 28–33 form an antiparallel β-hairpin while residues 35–40 of adjacent subunits form a parallel in-register β-sheet[55].

These oligomeric structures differ substantially from those of Aβ fibrils in which S2 and S3 segments each form in-register parallel β-sheets, each of which is antiparallel to the other[40, 42]. Although we have developed parallel β-barrel models with features similar to those of NMR-based models of fibrils, we do not favor those models as the predominant species because they are more complex, slightly less stable during molecular dynamics simulations, and less consistent with experimental results from studies of oligomers.

Toxicity

Our primary goal is to elucidate the assembly process and structures of Aβ oligomers underlying Alzheimer's disease. We have concentrated on Aβ42 because it is the most toxic

variant. The more common, but less toxic, Aβ40 is two residues shorter at the C-terminus due to its precursor being cleaved at a different site. Aβ42 forms paranuclei composed of five or six monomers[3, 5], hexamers and dodecamers[3], ADDLs (with typical molecular weights of four to nine monomers)[15, 32], and globulomers (12–16 subunits stabilized by fatty acids or detergents)[2]; whereas, Aβ40 peptide does not.

Side chains of E22 and D23 reside on opposite sides of β-sheets and do not interact in NMR-based models of preglobulomers[55] and fibrils[40, 41]; however, side chains of analogous residues in some more toxic Aβ mutants do appear to interact and covalent cross-linking of E22K and D23E side chains increases the toxicity of Aβ oligomers[37]. Thus, we have included models in which these side chains may interact.

Simplicity and Symmetry

We have concentrated on larger, more highly ordered models of relatively stable assemblies in which, when averaged over time, constituent peptides have few different conformations. There are several reasons for using this approach: 1) An NMR study concluded that Aβ oligomers form symmetrical micelle structures in which all peptides have the same conformation (Zagorski, MG, 2009 ICAD O2-06-06). 2) Aβ42 hexamers and dodecamers appear to be single molecular species, whereas smaller oligomers are not[3]. 3) All monomers have identical time-averaged conformations and interactions with neighboring subunits for the vast majority experimentally determined structures of protein assemblies composed of sequentially identical subunits[16]. This tendency may be related to the fact that typically, a protein's structure needs to be relatively static and ordered to be determined by X-ray diffraction or NMR. 4) Requiring all monomers to have identical conformations (or a small number of conformations) and identical interactions with their neighbors greatly simplifies the modeling process by reducing the number of plausible models; i.e. the number of possible explicit models of a large assembly is virtually infinite if all monomers can adopt different conformations. This constraint focuses the modeling efforts on those types of assemblies that can be experimentally tested by techniques such as X-ray crystallography and NMR spectroscopy. 5) We wish to develop models that will be useful for developing treatments for AD. Structure-based drug design works best for well-defined binding sites.

Our modeling efforts began with the hydrophobic S3 segment. A β-barrel is the simplest commonly-observed β motif for a relatively small core that has complete backbone H bonding and similar or identical conformations for all subunits. We have focused on hexameric β-barrels as basic building blocks for the following reasons: 1) There are numerous reports of hexameric (paranuclei[3, 5]) and dodecameric[25] (globulomer[2] and Aβ*56[35]) Aβ assemblies that may have developed from hexamers. 2) We find that S3 segments can form six-strand β-barrels that are very stable during molecular dynamic simulations. 3) This type of S3 β-barrel can form a hydrophobic core in which all of the polar backbone atoms of S3 (except at the ends) form H bonds to backbone atoms of adjacent strands, and in which all subunits can have identical conformations and interactions with neighboring subunits due to 3-fold symmetry around the axis of the barrel and 2-fold symmetry between the top and bottom halves of the antiparallel barrels. Edge effects prohibit these features for hexameric models that have more planar β-sheets. Models with parallel S3 barrels must have two subunit conformations because they have only 3-fold symmetry about the axis of the barrel.

The hydrophobic core is likely shielded from water by the more hydrophilic segments that precede it. Hydrogen/deuterium exchange studies indicate that these segments are more exposed to water, and likely more disordered than the core or S2 segments of fibrils. This situation creates a modeling dilemma; including all residues in the models may introduce errors and be misleading since no single model is likely to adequately represent the dynamic

nature of less ordered regions, but omitting residues may also introduce errors since even relatively disordered segments may be important in shielding the hydrophobic core from water and mutations in S1[8] and S2[3] segments affect the types of oligomers formed by Aβ peptides. Also, understanding structures of surface residues may be important for developing treatments that involve binding of drugs or antibodies to exposed residues. Thus, we have included all residues in our models and then used molecular dynamics simulations to analyze relative stabilities of each portion of a variety of models in which the cores and surrounding segments are modeled differently. We have modeled S2 as helical for some of our early stage soluble assemblies, but have modeled it as β in most larger assemblies. All NMR studies[40, 41, 55] conclude that the region at the end of S2 linking it to S3 forms a loop. These findings are consistent with the fact that four of the five residues in segment 25–29 (GSNKG) have a high propensity for coil and turn structure[10]. This region typically forms a turn and/or hinge region in our models. Most studies have found that most of S1 is highly dynamic and has little secondary structure; however, one study of fibrils does find some protection of amide groups of residues 3–5 and 8–14 in S1, indicating that it may not be entirely disordered[39]. When placed in a β structure, S1 exhibits an amphipathic pattern with predominately charged hydrophilic side chains on one side of the strand and hydrophobic and neutral side chains on the other side (Fig. 1A); however, residues 6–9 (HDSG) in the center of S1 are more consistent with a coiled or turn conformation[10] and residues 8–14 (GSYEVHH) form the initial part of a helix in some monomeric NMR structures[13, 50]. Although S1 was initially given a β-strand or β-hairpin conformation in most of our models, it is the most peripheral and least crucial segment in most models, and was typically the most dynamic region during MD simulations. It could have been classified as undefined in some cases.

Energetics

Preliminary models were constructed to be energetically sound; e.g., most hydrophobic side chains were buried, all charged groups except His6 were exposed to water and/or formed salt bridges, most residues were assigned regular secondary structures, side chains were assigned conformations commonly observed in crystal structures[45], and all polar backbone atoms of the central part of the putative S3 beta barrel formed hydrogen bonds. β-barrels were constructed to have conventional properties; i.e. strands were tilted relative to the axes of the barrels in the standard direction, with typical tilt angles and shear numbers[36]. Initial models were minimized with symmetry constraints using CHARMM[7]; i.e., a unit cell composed of one to three subunits is stipulated, the relationships among the unit cells of the complete assembly is defined by symmetry operations (e.g. three-fold symmetry about the z-axis and 2-fold symmetry about the y-axis for one subunit of an antiparallel hexamer, or two subunits of a dodecamer), and the minimization procedure maintains these symmetry relationships while minimizing the interactions both within and between unit cells. These minimized symmetric models were then examined to determine whether energetically favorable properties were maintained. If not, then the models were adjusted manually, the minimization step was repeated, and the models were reexamined. This process was repeated until no improvement was observed. Although these models were **not** based on results of MD simulations, MD simulations were used to refine and evaluate alternative models. The initial symmetric model was surrounded with water (or embedded in a phosphatidylethanolamine lipid bilayer with water and ions on each side for transmembrane models) and subjected to a 6 ns burst of unrestrained molecular dynamics simulation using Gromacs. A time averaged structure was calculated from the last 1 ns of the simulation and compared to the initial model. If portions of the simulated model deviated from the original symmetric model in a systemic manner (i.e., in the same direction in most of the subunits), these deviations were incorporated into another iteration of symmetric modeling. This process of symmetric modeling followed by unrestrained MD simulation was repeated,

typically three to four times for each hexameric model, until there was no substantial systematic deviation. The final models were then subjected to a longer 20 ns simulation to evaluate their stabilities. Hence overall, a model represents an average of 40ns of simulations. About fifty simulations beginning with differing initial conformations were performed for soluble Aβ42 assemblies. Root-mean-squared-deviations (RMSD) from the starting symmetric model were calculated as a function of time for both the entire structure and the S3 core to determine whether the models had approached equilibrium during the final simulation and to evaluate the stability of the model. Models with lower RMSD values were deemed to be more stable. Root-mean-squared-fluctuation (RMSF) values were calculated for each residue during the last 3 ns of each final simulation to determine which portions of the model were more dynamic or more stable. Segments with high RMSF values are proposed to have less ordered structures than those with low values. Averaged structures were calculated from the last 3 ns of the 20 ns simulations, and these structures were compared visually to the original models. As a control, simulations were also performed on three hexameric models constructed from different NMR-based models of Aβ40 fibrils.

We used targeted energy minimization with harmonic restraints on all the protein atoms towards the final conformation to explore growth of fibrils from dodecamers. Compared to the steered molecular dynamics, energy minimization better preserves secondary structure during the transition, although the sampling of the conformational space along the pathway is rather limited and proceeds without conformational conflicts for fairly straightforward transformations. To ensure a smooth transition with the lowest possible bias, the spring constant gradually increased from 0.001 to 10 kcal/mol/Å^2 over 1000 cycles (increased by about 1% every cycle). For every cycle, the structure was energy minimized for 100 steps using conjugate gradient and line search algorithm in NAMD[43] at the current value of the spring constant, and then for 100 more steps with no harmonic restraints to ensure better structure relaxation. The energy minimization was performed using CHARMM27 forcefield[7], rigid bonds to the hydrogens, 1 fs timestep, in vacuum with 14 Å cutoff on non-bonded interactions (smooth switching stated at 12 Å). To imitate the presence of the medium with high dielectric permeability (about 80), every 10 cycles the charges on the protein were adjusted proportional to the estimated exposure to the solvent using custom-written script in VMD[23]. The sequence of the energy minimizations, spring constant increase and charge adjustments was automated using external Tcl script. The results were visualized using VMD. Every 25th cycle of energy minimization was included into the Supplement Movie 2.

Molecular graphics images were produced using the UCSF Chimera package from the Resource for Biocomputing, Visualization, and Informatics at the University of California, San Francisco (supported by NIH P41 RR-01081); http://www.cgl.ucsf.edu/chimera.

RESULTS

Hexameric Models of Soluble and Transmembrane Assemblies

We have analyzed four categories of soluble hexameric Aβ42 models that can be described as antiparallel αβ-barrel, antiparallel ββ-barrel, parallel αβ-barrel, and parallel ββ-barrel models. In this nomenclature, the first Greek letter indicates the secondary structure of the S2 segment and the second that of S3 (see Fig. 1). The S1/S2 segments shield the outer walls of the hydrophobic S3-β-barrels from water in all of these models. (Figure 1 near here)

Within the antiparallel category, we considered three different models of S3-β barrels. These models differ primarily in the relative positions of the ascending and descending S3 strands as illustrated below for residues 28–42 (see supplement Fig. Sup1 for molecular images).

Side chains of bold residues are in the interior of the β-barrels. Type 3A models remained most stable during MD simulations and Type 3C models were least stable. Residues 41 and 42 participate more extensively in Type 3A barrels. This could explain why Aβ42 form hexamers while Aβ40 does not[5].

The antiparallel αβ-barrel model of Fig. 1B was constructed to have the following features: The boundaries of the putative helix are based on results of NMR studies of Aβ monomers in apolar solvents[13] and bound to lipid micelles[11]. A relatively hydrophobic face of the helix formed by Y10, H13, H14, L17, V18, F20, A21, V24, and G25 packs tightly next to the S3 β-barrel without overlapping side chains. The helices are antiparallel to and tilted in the same direction as the S3 strands of the same subunit in a manner typical of known αβ-barrel structures. The S2–S3 linker has a feasible conformation with energetically favorable torsion angles and side chain conformations. The first five residues of S1 (DAEFR denoted as S1a segment) have an extended conformation with the A2 and F4 side chains buried and interacting with hydrophobic residues V12 and F19 of the outer face of S2. S1a strands of adjacent antiparallel subunits are centered about an axis of two-fold symmetry and bind together in an antiparallel manner that increases the burial of the hydrophobic side chains and allows formations of several salt bridges among the charged side chains. The S2 helices' secondary structure was well maintained throughout MD, but the positions of the six helices shifted substantially in non-systemic ways; i.e., the directions of the shift differed from one subunit to another. These shifts increased the Root Mean Square Deviation (RMSD) of the entire protein from the original model to ~0.63 nm through most of the simulation (see supplement Fig. Sup2A). As expected, the N- and C-termini and S2–S3 linkers were the least stable regions (Fig. Sup2B). All of the charged groups, except for the E11 and E22 carboxyl groups, form salt bridges in the final minimized symmetric antiparallel model. Similarities of gross topologies of the antiparallel αβ-barrel and ββ-barrel models make it feasible that αβ-barrel structure forms first and then transitions into a ββ-barrel structure, as suggested by the greater abundance of α structure observed at the beginning of oligomer formation[9, 29, 30].

The S1/S2 segments were modeled several ways for the antiparallel ββ-barrel models. S2 β strands were modeled to form an antiparallel pair in which even numbered residues are exposed to water while the hydrophobic L17, F19, and A21 side chains pack next to the S3 strands. The orientation of the S2 and S3 strands within each subunit relative to one another is similar to that of NMR-based models of the fibrils (ref). The location of the antiparallel S2 pairs relative to the S3 core is constrained by the requirement that the axis of 2-fold symmetry through the S2 pair corresponds to an axis of 2-fold symmetry through the S3 core. The relative positions of two antiparallel S2 strands (residues 15–22) were modeled in the following two ways:

Type 2A) **Q**K**L**V**F**F**A**E→
EA**F**F**V**L**K**Q←

Type 2B) **Q**K**L**V**F**F**A**E→
EA**F**F**V**L**K**Q←

where bold residues are exposed.

The 2A type of antiparallel binding of an isolated residue 16–22 segment has been proposed previously[31] and was relatively stable in MD simulations in which the Type 3A barrel formed the core. Six S2 strands are insufficient to completely cover the surface of the S3 barrel. S1 strands fill the gaps on the outer surface formed between the three pairs of S2 strands in our models. The S1 strands were also modeled two ways: in model Type 1A residues 2–12 forms a continuous β strand that forms a β-hairpin with S2 (Fig. 1C), and in Type 1B residues 2–5 and 10–12 form a β hairpin. Hydrophobic side chains of residues of S1 (A2, F4, Y10, and V12) interact with the hydrophobic S3 core and a putative β turn connecting S1 to S2 strands is formed at H13 and H14 in both types of models.

Formation of hexamers is not dependent solely on S3 segments; e.g., a F19P[3] mutation in S2 eliminates ability of Aβ42 to form hexamers and reduces its toxicity, and a E3R[8] mutation in S1 increases the tendency of Aβ40 to form hexamer-sized oligomers and increases its toxicity. Some combinations of the different models for S1, S2, and S3 segments appear more stable than others during MD simulations. The most stable model has Types 1A, 2A, and 3A structures for S1, S2, and S3 (Fig. 1c and 2). Some alternative, albeit less stable, models (e.g. models with Type 3B antiparallel barrels, and parallel S3 barrels) and their stabilities are described in the supplement (Figs. Sup3–5).

The main advantages of the antiparallel over parallel models are that they are simpler (all monomers have identical conformations and identical interactions with neighboring subunits, whereas there are two monomeric conformations in the parallel models), and they are more consistent with experimental findings that Aβ oligomers form antiparallel β structures[9]. Stabilities during MD simulations of parallel and antiparallel models were comparable for ββ-barrel models, but the antiparallel S3 barrel was more stable for αβ-barrel models (see Supplement Fig. Sup4). Results of the MD simulations were comparable for the core region of antiparallel αβ-barrel and ββ-barrel models. As expected, the S3 β-barrel was the most stable region in all models, showing an exceptionally low root-mean-square deviation (RMSD) of 0.1 – 0.2 nm from the original model for the Type 3A antiparallel models and maintaining almost all of the H bonds between the strands.

We performed similar MD simulations on three hexamer models constructed from six adjacent subunits of NMR-based models of Aβ fibrils to determine how the stabilities of our β-barrel models compare to non-barrel models of hexamers based on other motifs. Two of these models had two parallel trimers related by two-fold symmetry about the axis of the fibril but different staggers of the S2 and S3 strands[42], and the third had three parallel dimers related by three-fold symmetry about the axis of the fibril[40] (see supplement Fig. Sup6). The most stable of these fibril-like models was the one with two-fold symmetry and a stagger of +2; the RMSD for the entire hexamer was ~ 0.1 nm greater than for the antiparallel ββ-barrel model described above, even though the most dynamic first eight residues of S1 were not included in the fibril-like model, and residues 32–39 of S3 had RMSD values about twice as great as those of our more stable β-barrel models. Conversely, the other model with 2-fold symmetry, with a stagger of −2, was the least stable: subunits actually drifted apart during the 20 ns simulations (results not shown). The major differences between these two models were the conformation of the S2–S3 loop and side chain interactions between S2 and S3 strands. Thus, the very different results obtained with initial models that have similar H-bonding patterns indicate that these types of MD simulations can distinguish stabilities among similar structural models, and that the stability is not determined solely by H-bonding. Finally, the model with 3 dimers related by 3-fold symmetry was also found to be unstable, with a RMSD from the starting model of ~ 1.5 nm at the end of a 20ns simulation and still increasing (supplement Fig Sup6). This model maintained most of its original parallel β-strand interactions, but new antiparallel interactions formed between a set of S2 and S3 strands within each dimer, and between S3 segments from two adjacent dimers (a semi-cylindrical 8-stranded β-sheet formed within two dimers with strand order S2-S2*S3-S3*S3-S3*S2-S2 where * indicates antiparallel interactions absent in the initial model). The decreased stability of the S3 segments in these fibril-based models is not surprising because not all edges of the S3 strands form intersubunit H-bonds; whereas, all S3 strands of our β-barrel models form intermolecular H-bonds on both sides. Thus, models with more complete H-bonding of backbone atoms tend to be more stable, as would be expected, but other factors such as loop conformations and side chain interactions also contribute to stability.

We also analyzed the stabilities of transmembrane Aβ42 hexamer assemblies in which the S3 β-barrel spans the bilayer while the S1/S2 segments extend into the aqueous phases. The main purpose of describing these simulations here is to analyze the stabilities of the S3 β-barrels in a hydrophobic environment in which they do not interact substantially with S1/S2 segments. The S3 β-barrel was very stable when S1–S2 segments were modeled either as a bundle of α-helices (see Fig. 1D) or as as a trible-stranded β-helix (not shown), indicating the conformation of the S1–S2 segments is not essential to the stability of the S3-barrel. These simulations indicate that the transmembrane S3 β-barrels are exceptionally stable for both antiparallel (see Fig. 2C) and parallel models (not shown). This increased stability relative to the soluble hexamers is probably due to the absence of water, which competes with backbone interactions for hydrogen bonds in soluble assemblies, and possibly absence of some backbone perturbing interactions with S1 and/or S2 segments.

Six-stranded β-barrels are rare. The presence of glycine at every fourth position throughout S3 (G29, G33, and G37) makes these β-barrel structures feasible for Aβ hexamers; the absence of a side chain at these positions eliminates steric clashes with other side chains, reduces the volume of side chains in the interior of the barrel, and allows the backbone to bend more than normally occurs in β-barrel structures. Replacing these glycines with alanine destabilizes the hexameric S3 β-barrel structure substantially during MD simulations (see Fig. Sup7 of supplement). Thus, these models in which odd numbered residues form the core of the hexameric S3-β-barrel are consistent with experimental findings that mutations I31E[8], G33A, G33I[18], G33L, and G37L[24] and oxidation of M35[6] reduce the tendency of Aβ42 peptides to form smaller oligomers (dimers to hexamers), reduce the toxicity of the peptides, and for G33 variants eliminate inhibition of long-term potentiation[18].

Annular protofibrils from hexamers

Electron microscopy using negative stain has identified structures called annular protofibrils[26, 33, 34]. An initial study of the Arctic (E22G) mutant of Aβ40 reported torus-shaped assemblies composed of 40–60 Aβ monomers with outer diameters of 7–10 nm and central pores with diameters of 1.5–2.0 nm[33]. A more recent study with Aβ42 observed that in early stages of assembly, the annular protofibrils appear to be formed by a ring of spherical particles, each of which has a diameter of 3–5 nm[26]. Portions of these 'beaded' structures resemble portions of short linear protofibrils that have been proposed to be formed by interactions between paranuclei[5]. After several days of incubation, the spheres disappear and the rings have relatively smooth continuous surfaces.

Here we describe a relatively simple way that the antiparallel hexamers described above could assemble to form a `beaded' annular protofibril and then merge to form a continuous annular protofibril. The simplest way to form a beaded protofibril from the antiparallel hexamers described above is to assemble the hexamers into a P62 hexagonal lattice with an axis of two-fold symmetry at the region of closest contact between adjacent hexamers and an axis of 6-fold symmetry through the center of the torus, both of which are parallel to the axis of three-fold symmetry of the β-barrel (Fig. 3A). The three outer S1–S2 sheets of the ββ-barrel model of Fig. 1B form a structure with triangular-shaped cross-section. The mid-region of each outer sheet has a hydrophobic patch formed by two F18 and two V20 side chains located in the middle of the S2 segments. These are the only exposed hydrophobic residues on the surface of the ββ-barrel hexamers. These hexamers were packed in the P62 lattices so that F18 and V20 are buried and interact with their counterparts from an adjacent hexamer near an axis of two-fold symmetry (Fig. 3B). These patches are surrounded by a series of charged side chains that form several salt bridges between hexamers in the lattice models. The central pore around the six-fold axis is formed by the hydrophilic `corners' of the equilateral triangles.

The hexamers may slowly merge to form the smooth annular protofibril. In the beaded model, one third of the S1–S2 β-hairpins are on the interior of the assembly and two thirds are on the exterior. An initial step in the merging process may be the formation of an interior 24-stranded antiparallel β-barrel by the interior S1–S2 hairpins. This step would remove residues positioned between the hexameric S3 barrels. Next, the six S3 β-barrels may split apart between two strands (as was observed during MD simulations of some of the less stable models), flatten, and then join S3 strands of an adjacent hexamer to form a continuous 36-stranded antiparallel S3 β-barrel. Likewise, the exterior S1–S2 hairpins may interact to form an exterior 48-stranded antiparallel β-barrel (a movie illustrating this transition is in the supplement). Thus the smooth model comprises three concentric antiparallel β-barrels with the hydrophobic S3 barrel sandwiched between S1–S2 barrels (see Fig. 3D). The shear number of each barrel equals the number of strands. The diameter to the backbone wall of each barrel is ~ 4.3, 6.3, and 8.3 nm, leaving a gap of ~ 1.0 nm between barrels to be occupied by side chain and backbone atoms. The more hydrophobic faces of the S1 and S2 strands are oriented toward the central S3 barrel while the more charged faces are exposed to water inside the central pore or on the outer surface (Fig. 3 E and F). The smooth annular protofibril model retains only the 6-fold symmetry about the central axis and 2-fold symmetry from top to bottom. Thus, unlike the beaded hexamer of hexamer models, every subunit does not have the same conformation; rather, there are three subunit conformations, each of which occurs twelve times in the 36mer. The large antiparallel β-barrels of these models are consistent with two experimental findings. Antibodies that recognize these annular protofibrils but not monomeric Aβ, also recognize the heptameric α-hemolysin channel protein[26], which has no significant sequence homology but does have a large 14-stranded antiparallel β-barrel motif, suggesting these antibodies recognize the backbone motif rather than a specific sequence[49]. A comparison of FTIR spectroscopic signals produced by Aβ42 oligomers composed of 8–38 peptides to those produced by proteins of known structure found the most similar signal was produced by OmpF[9], a transmembrane porin channel with a large 16-stranded antiparallel β-barrel[12].

The outer diameters of the smooth and beaded models are ~9 and 10 nm, consistent with the size reported for some annular protofibrils: Lashuel et al[33] reported outer diameters of 8–10 nm of rings composed of 40–60 subunits. The study of Kayed et al[26] reported a larger range of sizes, and while rings composed of six beads were observed, rings with more than six beads were also common. Thus, much of the variation in the size of the protofibrils could be caused by variations in the number of hexamers forming the ring and/or the binding of additional Aβ42 subunits to the hexamers, as proposed below for formation of dodecamers.

MD simulations indicate that `smooth' models are substantially more stable than the `beaded' models (see supplement Fig. Sup8). The all atom RMSD from the starting symmetric beaded 36mer assembly at the end of a 20 ns simulation was 0.6 – 0.7 nm and the assembly has ~ 1132 non-water hydrogen bonds. In contrast, the RMSD of the smooth assembly was ~0.4 nm and there were ~ 1296 non-water H bonds. This increased stability may be attributed to numerous backbone H bonds formed between hexamers in the smooth models that are not present in the beaded models, and perhaps to the more conventional nature of the β barrels.

We have constructed similar hexamer-of-hexamers models from models with Type 3B ββ-barrels, antiparallel αβ-barrels, and parallel ββ-barrels (see supplement Fig Sup9); however, these models tend to be less stable and/or less consistent with the finding that soluble oligomers have antiparallel secondary structure.

Dodecamers

The dodecamer model considered here adds six additional subunits to the antiparallel ββ-barrel model described above (see Fig. 4). These models are candidates for the Aβ*56

assemblies[3, 35]. A recent study[3] reported the presence of Aβ42 dimers, tetramers, hexamers, decamers, and dodecamers, with hexamers and dodecamers being the most prevalent species. Interestingly, they did not observe odd numbered oligomers, octamers, or oligomers larger than dodecamers. This category of models has three concentric layers; the inner core is a six-stranded Type 3A S3 β-barrel, the second or middle layer is a twelve stranded β barrel formed by six S2 and six S3 strands, and the outer layer has six S2 strands and twelve S1 strands. There are two types of monomeric subunit structures in these models, which we call the core subunits and the peripheral subunits. Conformations of the S2 and S3 segments of the core subunits are about the same as in the hexameric model; S3 segments form the innermost six-stranded β-barrel and S2 segments form part of a surrounding 12-stranded β-barrel; however, the S1 segments are shifted to the outer surface, or third layer, where they cover part of the S2 strands of the core subunits. The peripheral subunits also have conformations similar to those of the hexameric models in that the S1 and S2 segments form β-hairpins that comprise part of a surface layer (third layer in the dodecamer) while the S3 segments form part of the mid-layer twelve-stranded β-barrel.

In developing the dodecameric models, we did not examine all of the alternative possibilities for relative positions of S1, S2, and S3 segments or alternative conformations of S1 segments that were evaluated in the hexameric models. Thus, we are not confident that the model illustrated in Fig. 4 is better than alternatives. Nonetheless, the MD simulations of this model do indicate that the basic structural motif is relatively stable. The internal structures of the inner 6-stranded β-barrel remained very stable during 20 ns MD simulations (RMSD ~ 0.14 nm), the mid-layer 12-stranded β-barrel was moderately stable (RMSD ~ 0.25 nm), and the remaining segments were less stable (RMSD ~ 0.39 nm for entire protein, see supplement Fig. Sup10). The internal structure of the three outer β-sheets formed by antiparallel pairs of S1/S2 β-hairpins of the peripheral subunits remained fairly stable, but the positions of these sheets drifted in different ways for the three sheets during MD simulations. The S1 strands from the core subunits were dynamic and unstable.

Growth of fibrils from βββ-dodecamers

It has recently been proposed that Aβ42 fibrils can develop from Aβ42 dodecamers[3]. We have explored the possibility that ββ-barrel hexamers or βββ-barrel dodecamers could act as seeds from which fibrils grow. Some NMR-based models of fibrils[41] have the following features in common with these β-barrel models: 1) the hydrophobic cores of both are formed by S3 strands, 2) the S3 strands on opposite sides of the structures are oriented in opposite directions and are related by 2-fold symmetry, and 3) S2 and S3 strands are oriented relative to each other in a similar way within each subunit. A major difference is that the β-sheets of the fibrils are parallel and relatively planar (with some twist), whereas those of the β-barrels are antiparallel and cylindrical. The growth of a double-layered parallel fibril structure from an antiparallel β-barrel could be initiated by splitting the β-barrel between adjacent subunits and parallel binding of Aβ subunits to these unpaired edge strands. The βββ-barrel dodecamer models (Fig. 4) already have S3 strands of the mid-layer β-barrel positioned parallel to S3 strands of the core barrel. Thus, parallel S3 β-sheets may be initiated by formation of backbone H bonds between these strands (Fig. 6). Once this occurs, additional Aβ subunits may bind to the exposed unpaired edge strands to extend the parallel sheets. We positioned a series of antiparallel Aβ dimers next to the βββ-dodecamers and then used targeted energy minimization to form fibril-like β structures from these assemblies to examine the feasibility of such transitions (Fig. 5 and supplement movie 2). The S2 and S3 segments of the dimers were assigned helical structures to ensure that the structures of these additional peptides differed substantially from those of the final structures. These simulations progressed very smoothly, with no apparent structural conflicts or unrealistic disruptions of the secondary structure. The simulation illustrated in Supplement Movie 2

used six intermediate conformations; however, additional simulations using only the first and last conformations with no intermediate conformations also proceeded well in both directions. Although some aspects of these simulations are not realistic representations of the actual process, they demonstrate the feasibility of growth of a fibril structure from the βββ-barrel dodecamer. The β strands in the parallel β sheets developed from the βββ-barrel models are more tilted than those of the NMR-based structures due to the tilt of the strands in the β-barrels (Fig. 5C). We suspect that the sheets would eventually shift to the fibril type structure in which all adjacent strands are in register.

DISCUSSION

The central hypothesis of our models of both soluble and membrane-bound (see accompanying manuscript) oligomers of Aβ is that the hydrophobic C-terminus third of the peptides (S3) assemble to form six-stranded β-barrels. The exceptional stability of hexameric S3 β-barrels during MD simulations appears to be an intrinsic property that is not highly dependent upon a precise environment; i.e., they are stable when surrounded by α-helices, β-sheets, or membrane lipids. The S1/S2 segments of soluble hexamers are substantially less stable, and may fluctuate among different conformations that may vary with time and environment. These theoretical findings are consistent with experimental results[9, 27, 28, 55, 56] indicating that S3 segments of Aβ oligomers have relatively ordered β structures that are inaccessible to water, whereas the S2 and especially S1 segments are less ordered and more accessible.

The text describes the specific symmetric models that were most stable during MD simulations. These *simplified* models serve to illustrate the general concepts and motifs. However in some cases, the stabilities of these models were only slightly better than those of alternatives. We suspect that actual assemblies will be more complicated than those described here; e.g., some S3 β-barrel assemblies could be composed of a mixture of Type 3A, 3B, and 3C antiparallel or parallel and antiparallel S3 strands, and some barrels could have more than six S3 strands. The surfaces formed by S1 and S2 segments are even more dynamic and even the secondary structures of these segments may differ between or within a particular assembly. These abilities of the general motif to accommodate different peptide conformations should be entropically favorable. Thus, our models should not be interpreted too precisely; the most general version of the model is simply that the hydrophobic core of Aβ42 hexamers may be a six-stranded β-barrel which is shielded from water by S1 and S2 segments.

We have illustrated three types of processes by which these hexamers may lead to larger assemblies; the proposed process to form annular protofibrils involves self-association and then merging of hexamers, the process to form dodecamers involves radial addition of peptides to the hexameric core, and the process to form fibrils involves linear growth of the assembly from one side of an initial dodecamer. We have also extended this hypothesis to models of membrane-bound Aβ assemblies similar to the annular protofibril models in which six hexamers merge together to form a channel with a 36-stranded antiparallel S3 β-barrel, and have modeled how some drugs inhibit Aβ toxicity by binding in the pore of these channels (see accompanying manuscript). This hypothesis can also be extended to the Prion Protein since its hydrophobic segment contains the residues at every other position essential for the motif; i.e., GxLxGxMxG for PrP and GxIxGxMxG for Aβ where X represents a hydrophobic residue (2007 Biophysical Society Meeting abs 2667).

Our finding that Type 3A antiparallel S3 β-barrel models are more stable than alternatives may explain why Aβ42 forms hexamers and dodecamers, whereas Aβ40 does not. This increased stability may be due to residues 41 and 42 forming part of the Type 3A S3 barrel

and the binding of the C-terminus carboxyl group of residue 42 to the K28 side chain of the adjacent subunit in Type 3A models. The fact that the hexamers and dodecamers are highly toxic may in turn explain why Aβ42 is more toxic than Aβ40. To our knowledge, ours are the only models to explain the importance of the glycine at every 4th position, and why even conservative substitutions at these positions[18, 24] and oxidation of M35[6] and a E31I mutation[8] inhibit formation of hexameric-sized oligomers and reduce toxicity of the peptides.

The first major unresolved question raised by these models is whether or not any of the proposed assemblies actually exists. The major impediments to answering this question experimentally are polymorphism (too many different types of oligomers/assemblies present in the preparation), inherent disorder (the N-terminus of Aβ is too disordered to be solved in fibrils, and some oligomers appear to be much less ordered than fibrils), aggregation into higher order assemblies that complicates solution NMR, and morphing to different structures over time. One plausible approach would be to synthesize Aβ homologs designed to stabilize specific structural models and to inhibit aggregation of these structures into larger assemblies. For example, the number of peptides within an assembly could be limited to hexamers by tethering six peptides together in a manner permitted by the models; aggregation of hexamers could be inhibited by mutating surface hydrophobic residues (such as F18 and V20) proposed to be involved in aggregation to hydrophilic residues that repel one another; proposed secondary structures could be stabilized by mutating residues that disfavor the structure to residues that favor the structure. Some experimental studies support a hypothesis in which Tyr10 side chains of two Aβ monomers cross-link under oxidizing conditioning, which may result from the binding of copper to Aβ peptides. This cross-linking appears to increase the toxicity of the assemblies, and may explain the exceptional stability of some Aβ dimers[38]. Although we have not used this information in developing our models, Tyr 10 side chains of adjacent dimers are near each other in the ββ-barrel model of Fig 1B and are also near His 13 and His 14 of the adjacent subunit. These residues may form part of a copper binding site that produces hydrogen peroxide, which in turn generates tyrosyl radicals which then crosslink[14, 38]. Thus, this type of cross-linking could stabilize these structures.

The second major question is which, if any, of the proposed types of assemblies are responsible for AD. It is currently unclear whether the neurotoxicity of oligomers is due to soluble or membrane-bound assemblies, and in either case which specific assemblies are involved. It is possible that different types of assemblies may cause neurological damage through different mechanisms. Again, synthesizing Aβ homologs that form unique types of assemblies could be useful in resolving these questions.

Supplementary Material

Refer to Web version on PubMed Central for supplementary material.

Acknowledgments

This work was supported by the Intramural Research Program of the NIH, National Cancer Institute, Center for Cancer Research. We thank Adina Milac and Sijung Yun for comments and Sijung Yun for making the Movie 1 of the supplement for transitions from beaded to smooth annular protofibril and Robert Tycko for providing coordinates of Aβ40 fibril models.

Abbreviations

Aβ (amyloid beta)

AD (Alzheimer's disease)

MD (molecular dynamics)

Reference List

1. Arispe N. Architecture of the Alzheimer's A beta P ion channel pore. J Membr Biol. 2004; 197:33–48. [PubMed: 15014916]
2. Barghorn S, Nimmrich V, Striebinger A, Krantz C, Keller P, Janson B, Bahr M, Schmidt M, Bitner RS, Harlan J, Barlow E, Ebert U, Hillen H. Globular amyloid beta-peptide oligomer - a homogenous and stable neuropathological protein in Alzheimer's disease. J Neurochem. 2005; 95:834–847. [PubMed: 16135089]
3. Bernstein SL, Dupuis NF, Lazo ND, Syttenbach T, Condron MM, Bitan G, Teplow DB, Shea J-E, Ruotolo BT, Robinson CV, Bowers MT. Amyloid-beta protein oligomerization and the importance of tetramers and dodecamers in the aetiology of Alzheimer's disease. Nature Chemistry. 2009 DOI: 10.1038/NCHEM.247.
4. Bharadwaj PR, Dubey AK, Masters CL, Martins RN, Macreadie IG. Abeta aggregation and possible implications in Alzheimer's disease pathogenesis. J Cell Mol Med. 2009; 13:412–421. [PubMed: 19374683]
5. Bitan G, Kirkitadze MD, Lomakin A, Vollers SS, Benedek GB, Teplow DB. Amyloid beta -protein (Abeta) assembly: Abeta 40 and Abeta 42 oligomerize through distinct pathways. Proc Natl Acad Sci U S A. 2003; 100:330–335. [PubMed: 12506200]
6. Bitan G, Tarus B, Vollers SS, Lashuel HA, Condron MM, Straub JE, Teplow DB. A molecular switch in amyloid assembly: Met(35) and amyloid beta-protein oligomerization. Journal of the American Chemical Society. 2003; 125:15359–15365. [PubMed: 14664580]
7. Brooks BR, Brooks CL III, Mackerell AD Jr. Nilsson L, Petrella RJ, Roux B, Won Y, Archontis G, Bartels C, Boresch S, Caflisch A, Caves L, Cui Q, Dinner AR, Feig M, Fischer S, Gao J, Hodoscek M, Im W, Kuczera K, Lazaridis T, Ma J, Ovchinnikov V, Paci E, Pastor RW, Post CB, Pu JZ, Schaefer M, Tidor B, Venable RM, Woodcock HL, Wu X, Yang W, York DM, Karplus M. CHARMM: the biomolecular simulation program. J Comput Chem. 2009; 30:1545–1614. [PubMed: 19444816]
8. Brorsson AC, Bolognesi B, Tartaglia GG, Shammas SL, Favrin G, Watson I, Lomas DA, Chiti F, Vendruscolo M, Dobson CM, Crowther DC, Luheshi LM. Intrinsic determinants of neurotoxic aggregate formation by the amyloid beta peptide. Biophys J. 2010; 98:1677–1684. [PubMed: 20409489]
9. Cerf E, Sarroukh R, Tamamizu-Kato S, Breydo L, Derclaye S, Dufrene YF, Narayanaswami V, Goormaghtigh E, Ruysschaert JM, Raussens V. Antiparallel beta-sheet: a signature structure of the oligomeric amyloid beta-peptide. Biochem J. 2009; 421:415–423. [PubMed: 19435461]
10. Chou PY, Fasman GD. Empirical Predictions of Protein Conformation. Annual Review of Biochemistry. 1978; 47:251–276.
11. Coles M, Bicknell W, Watson AA, Fairlie DP, Craik DJ. Solution structure of amyloid beta-peptide(1–40) in a water-micelle environment. Is the membrane-spanning domain where we think it is? Biochemistry. 1998; 37:11064–11077. [PubMed: 9693002]
12. Cowan SW, Schirmer T, Rummel G, Steiert M, Ghosh R, Pauptit RA, Jansonius JN, Rosenbusch JP. Crystal-Structures Explain Functional-Properties of 2 Escherichia-Coli Porins. Nature. 1992; 358:727–733. [PubMed: 1380671]
13. Crescenzi O, Tomaselli S, Guerrini R, Salvadori S, D'Ursi AM, Temussi PA, Picone D. Solution structure of the Alzheimer amyloid beta-peptide (1–42) in an apolar microenvironment. Similarity with a virus fusion domain. Eur J Biochem. 2002; 269:5642–5648. [PubMed: 12423364]
14. Curtain CC, Ali F, Volitakis I, Cherny RA, Norton RS, Beyreuther K, Barrow CJ, Masters CL, Bush AI, Barnham KJ. Alzheimer's disease amyloid-beta binds copper and zinc to generate an allosterically ordered membrane-penetrating structure containing superoxide dismutase-like subunits. J Biol Chem. 2001; 276:20466–20473. [PubMed: 11274207]

15. Gong Y, Chang L, Viola KL, Lacor PN, Lambert MP, Finch CE, Krafft GA, Klein WL. Alzheimer's disease-affected brain: presence of oligomeric A beta ligands (ADDLs) suggests a molecular basis for reversible memory loss. Proc Natl Acad Sci U S A. 2003; 100:10417–10422. [PubMed: 12925731]

16. Goodsell DS, Olson AJ. Structural symmetry and protein function. Annual Review of Biophysics and Biomolecular Structure. 2000; 29:105–153.

17. Hardy JA, Higgins GA. Alzheimer's disease: the amyloid cascade hypothesis. Science. 1992; 256:184–185. [PubMed: 1566067]

18. Harmeier A, Wozny C, Rost BR, Munter LM, Hua HQ, Georgiev O, Beyermann M, Hildebrand PW, Weise C, Schaffner W, Schmitz D, Multhaup G. Role of Amyloid-beta Glycine 33 in Oligomerization, Toxicity, and Neuronal Plasticity. Journal of Neuroscience. 2009; 29:7582–7590. [PubMed: 19515926]

19. Harper JD, Wong SS, Lieber CM, Lansbury PT. Observation of metastable A beta amyloid protofibrils by atomic force microscopy. Chemistry & Biology. 1997; 4:119–125. [PubMed: 9190286]

20. Hartley DM, Walsh DM, Ye CPP, Diehl T, Vasquez S, Vassilev PM, Teplow DB, Selkoe DJ. Protofibrillar intermediates of amyloid beta-protein induce acute electrophysiological changes and progressive neurotoxicity in cortical neurons. Journal of Neuroscience. 1999; 19:8876–8884. [PubMed: 10516307]

21. Hoshi M, Sato M, Matsumoto S, Noguchi A, Yasutake K, Yoshida N, Sato K. Spherical aggregates of beta-amyloid (amylospheroid) show high neurotoxicity and activate tau protein kinase I/glycogen synthase kinase-3 beta. Proceedings of the National Academy of Sciences of the United States of America. 2003; 100:6370–6375. [PubMed: 12750461]

22. Huang TH, Yang DS, Plaskos NP, Go S, Yip CM, Fraser PE, Chakrabartty A. Structural studies of soluble oligomers of the Alzheimer beta-amyloid peptide. J Mol Biol. 2000; 297:73–87. [PubMed: 10704308]

23. Humphrey W, Dalke A, Schulten K. VMD: visual molecular dynamics. J Mol Graph. 1996; 14:33–38. [PubMed: 8744570]

24. Hung LW, Ciccotosto GD, Giannakis E, Tew DJ, Perez K, Masters CL, Cappai R, Wade JD, Barnham KJ. Amyloid-beta Peptide (A beta) Neurotoxicity Is Modulated by the Rate of Peptide Aggregation: A beta Dimers and Trimers Correlate with Neurotoxicity. Journal of Neuroscience. 2008; 28:11950–11958. [PubMed: 19005060]

25. Jang H, Arce FT, Capone R, Ramachandran S, Lal R, Nussinov R. Misfolded Amyloid Ion Channels Present Mobile beta-Sheet Subunits in Contrast to Conventional Ion Channels. Biophys J. 2009; 97:3029–3037. [PubMed: 19948133]

26. Kayed R, Pensalfini A, Margol L, Sokolov Y, Sarsoza F, Head E, Hall J, Glabe C. Annular Protofibrils Are a Structurally and Functionally Distinct Type of Amyloid Oligomer. Journal of Biological Chemistry. 2009; 284:4230–4237. [PubMed: 19098006]

27. Kheterpal I, Chen M, Cook KD, Wetzel R. Structural differences in A beta amyloid protofibrils and fibrils mapped by hydrogen exchange - Mass spectrometry with on-line proteolytic fragmentation. Journal of Molecular Biology. 2006; 361:785–795. [PubMed: 16875699]

28. Kheterpal I, Lashuel HA, Hartley DM, Wlaz T, Lansbury PT, Wetzel R. A beta protofibrils possess a stable core structure resistant to hydrogen exchange. Biochemistry. 2003; 42:14092–14098. [PubMed: 14640676]

29. Kirkitadze MD, Condron MM, Teplow DB. Identification and characterization of key kinetic intermediates in amyloid beta-protein fibrillogenesis. J Mol Biol. 2001; 312:1103–1119. [PubMed: 11580253]

30. Kirkitadze MD, Li H, Condron MM, Zagorski MG, Teplow DB. Formation of an alpha-helix-containing, oligomeric intermediate is an obligatory step in amyloid beta-protein fibrillogenesis. Biophysical Journal. 2001; 80:174A.

31. Klimov DK, Thirumalai D. Dissecting the assembly of A beta(16–22) amyloid peptides into antiparallel beta sheets. Structure. 2003; 11:295–307. [PubMed: 12623017]

32. Lambert MP, Barlow AK, Chromy BA, Edwards C, Freed R, Liosatos M, Morgan TE, Rozovsky I, Trommer B, Viola KL, Wals P, Zhang C, Finch CE, Krafft GA, Klein WL. Diffusible, nonfibrillar

ligands derived from A beta(1–42) are potent central nervous system neurotoxins. Proceedings of the National Academy of Sciences of the United States of America. 1998; 95:6448–6453. [PubMed: 9600986]

33. Lashuel HA, Hartley D, Petre BM, Walz T, Lansbury PT Jr. Neurodegenerative disease: amyloid pores from pathogenic mutations. Nature. 2002; 418:291. [PubMed: 12124613]
34. Lashuel HA, Lansbury PT Jr. Are amyloid diseases caused by protein aggregates that mimic bacterial pore-forming toxins? Q Rev Biophys. 2006; 39:167–201. [PubMed: 16978447]
35. Lesne S, Koh MT, Kotilinek L, Kayed R, Glabe CG, Yang A, Gallagher M, Ashe KH. A specific amyloid-beta protein assembly in the brain impairs memory. Nature. 2006; 440:352–357. [PubMed: 16541076]
36. Liu WM. Shear numbers of protein beta-barrels: Definition refinements and statistics. Journal of Molecular Biology. 1998; 275:541–545. [PubMed: 9466929]
37. Masuda Y, Uemura S, Ohashi R, Nakanishi A, Takegoshi K, Shimizu T, Shirasawa T, Irie K. Identification of Physiological and Toxic Conformations in A beta 42 Aggregates. Chembiochem. 2009; 10:287–295. [PubMed: 19115328]
38. Naylor R, Hill AF, Barnham KJ. Neurotoxicity in Alzheimer's disease: is covalently crosslinked A beta responsible? European Biophysics Journal with Biophysics Letters. 2008; 37:265–268. [PubMed: 18064449]
39. Olofsson A, Lindhagen-Persson M, Vestling M, Sauer-Eriksson AE, Ohman A. Quenched hydrogen/deuterium exchange NMR characterization of amyloid-beta peptide aggregates formed in the presence of Cu2+ or Zn2+ Febs Journal. 2009; 276:4051–4060. [PubMed: 19549187]
40. Paravastu AK, Leapman RD, Yau WM, Tycko R. Molecular structural basis for polymorphism in Alzheimer's beta-amyloid fibrils. Proceedings of the National Academy of Sciences of the United States of America. 2008; 105:18349–18354. [PubMed: 19015532]
41. Paravastu AK, Petkova AT, Tycko R. Polymorphic fibril formation by residues 10–40 of the Alzheimer's beta-amyloid peptide. Biophys J. 2006; 90:4618–4629. [PubMed: 16565054]
42. Petkova AT, Yau WM, Tycko R. Experimental constraints on quaternary structure in Alzheimer's beta-amyloid fibrils. Biochemistry. 2006; 45:498–512. [PubMed: 16401079]
43. Phillips JC, Braun R, Wang W, Gumbart J, Tajkhorshid E, Villa E, Chipot C, Skeel RD, Kale L, Schulten K. Scalable molecular dynamics with NAMD. J Comput Chem. 2005; 26:1781–1802. [PubMed: 16222654]
44. Podlisny MB, Ostaszewski BL, Squazzo SL, Koo EH, Rydell RE, Teplow DB, Selkoe DJ. Aggregation of Secreted Amyloid Beta-Protein Into Sodium Dodecyl Sulfate-Stable Oligomers in Cell-Culture. Journal of Biological Chemistry. 1995; 270:9564–9570. [PubMed: 7721886]
45. Ponder JW, Richards FM. Tertiary Templates for Proteins - Use of Packing Criteria in the Enumeration of Allowed Sequences for Different Structural Classes. Journal of Molecular Biology. 1987; 193:775–791. [PubMed: 2441069]
46. Quist A, Doudevski I, Lin H, Azimova R, Ng D, Frangione B, Kagan B, Ghiso J, Lal R. Amyloid ion channels: a common structural link for protein-misfolding disease. Proc Natl Acad Sci U S A. 2005; 102:10427–10432. [PubMed: 16020533]
47. Rahimi F, Shanmugam A, Bitan G. Structure-function relationships of prefibrillar protein assemblies in Alzheimer's disease and related disorders. Current Alzheimer Research. 2008; 5:319–341. [PubMed: 18537546]
48. Roher AE, Palmer KC, Yurewicz EC, Ball MJ, Greenberg BD. Morphological and Biochemical Analyses of Amyloid Plaque Core Proteins Purified from Alzheimer-Disease Brain-Tissue. Journal of Neurochemistry. 1993; 61:1916–1926. [PubMed: 8229002]
49. Song L, Hobaugh MR, Shustak C, Cheley S, Bayley H, Gouaux JE. Structure of staphylococcal alpha-hemolysin, a heptameric transmembrane pore. Science. 1996; 274:1859–1866. [PubMed: 8943190]
50. Tomaselli S, Esposito V, Vangone P, van Nuland NA, Bonvin AM, Guerrini R, Tancredi T, Temussi PA, Picone D. The alpha-to-beta conformational transition of Alzheimer's Abeta-(1–42) peptide in aqueous media is reversible: a step by step conformational analysis suggests the location of beta conformation seeding. Chembiochem. 2006; 7:257–267. [PubMed: 16444756]

51. Walsh DM, Lomakin A, Benedek GB, Condron MM, Teplow DB. Amyloid beta-protein fibrillogenesis - Detection of a protofibrillar intermediate. Journal of Biological Chemistry. 1997; 272:22364–22372. [PubMed: 9268388]

52. Walsh DM, Tseng BP, Rydel RE, Podlisny MB, Selkoe DJ. The oligomerization of amyloid beta-protein begins intracellularly in cells derived from human brain. Biochemistry. 2000; 39:10831–10839. [PubMed: 10978169]

53. Westlind-Danielsson A, Arnerup G. Spontaneous in vitro formation of supramolecular beta-amyloid structures, “betaamy balls”, by beta-amyloid 1–40 peptide. Biochemistry. 2001; 40:14736–14743. [PubMed: 11732892]

54. Williams AD, Sega M, Chen ML, Kheterpal I, Geva M, Berthelier V, Kaleta DT, Cook KD, Wetzel R. Structural properties of A beta protofibrils stabilized by a small molecule. Proceedings of the National Academy of Sciences of the United States of America. 2005; 102:7115–7120. [PubMed: 15883377]

55. Yu LP, Edalji R, Harlan JE, Holzman TF, Lopez AP, Labkovsky B, Hillen H, Barghorn S, Ebert U, Richardson PL, Miesbauer L, Solomon L, Bartley D, Walter K, Johnson RW, Hajduk PJ, Olejniczak ET. Structural Characterization of a Soluble Amyloid beta-Peptide Oligomer. Biochemistry. 2009; 48:1870–1877. [PubMed: 19216516]

56. Zhang A, Qi W, Good TA, Fernandez EJ. Structural Differences between A beta(1–40) Intermediate Oligomers and Fibrils Elucidated by Proteolytic Fragmentation and Hydrogen/Deuterium Exchange. Biophysical Journal. 2009; 96:1091–1104. [PubMed: 19186145]

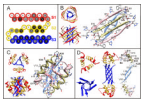

Figure 1.

Nomenclature and hexameric models of Aβ42. A) Aβ42 sequence divided into three segments of equal length: S1 (red), S2 (yellow), and S3 (blue). The background within each circle indicates the polarity of the residue: black = hydrophobic, dark gray = slightly hydrophobic to ambivalent, light gray = ambivalent to slightly hydrophilic, white = hydrophilic. B) Ribbon representation of an antiparallel ββ-barrel hexamer in which the S1 (red), S2 (yellow), and S3 (blue) segments form β-strands. A top view down the axis of the barrel of all six subunits is in the upper left corner, a side view (rotated by 90□ about the X axis relative to top view) is in the lower left corner, and the larger image is a side view of two subunits viewed along an axis of 2-fold symmetry with side chains of S1 and S2 colored by atom. Some residues of one subunit are labeled with bold labels for charged side chains. C) An αβ-barrel model similar to the model in B except that the latter part of S1 and most of S2 form an α-helix. D) Transmembrane model in which the blue S3 antiparallel β-barrel spans the bilayer and S1–S2 helices extend into the aqueous phases on each side of the membrane. Views down the axis of the structure are shown on the left for aqueous phase (top) and transmembrane (bottom) regions. The middle shows a side view of the hexamer, and a dimer with side chains is shown on the right. All three models have type 3A S3 β-barrels. Side chain color code: blue = nitrogen, red = oxygen, gray = carbon, white = hydrogen.

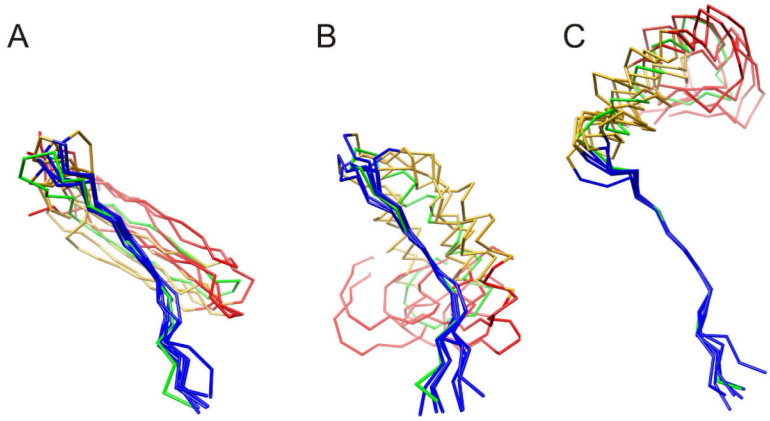

Figure 2.

MD results for three hexameric models of Aβ42 with Type 3A β-barrels. The multicolored backbone Cα traces illustrate superimposed results for six monomers averaged over the last 3 ns of a 20 ns MD simulation and the green traces illustrate the original model. The central portion of the S3 barrels of the simulated models were first fit to that of the original model for all subunits simultaneously, and then the subunits were superimposed by reversing the symmetry operations used to generate the original model. A) The ββ-barrel model, B) the αβ-barrel model, and C) the transmembrane model. Note that the central portion of the blue S3 segments did not deviate much from the original model, and that deviations of the more exposed S1 (red) and S2 (yellow) segments were substantially greater. See supplement Fig. Sup2 for RMSD vs time and RMSF vs residue plots.

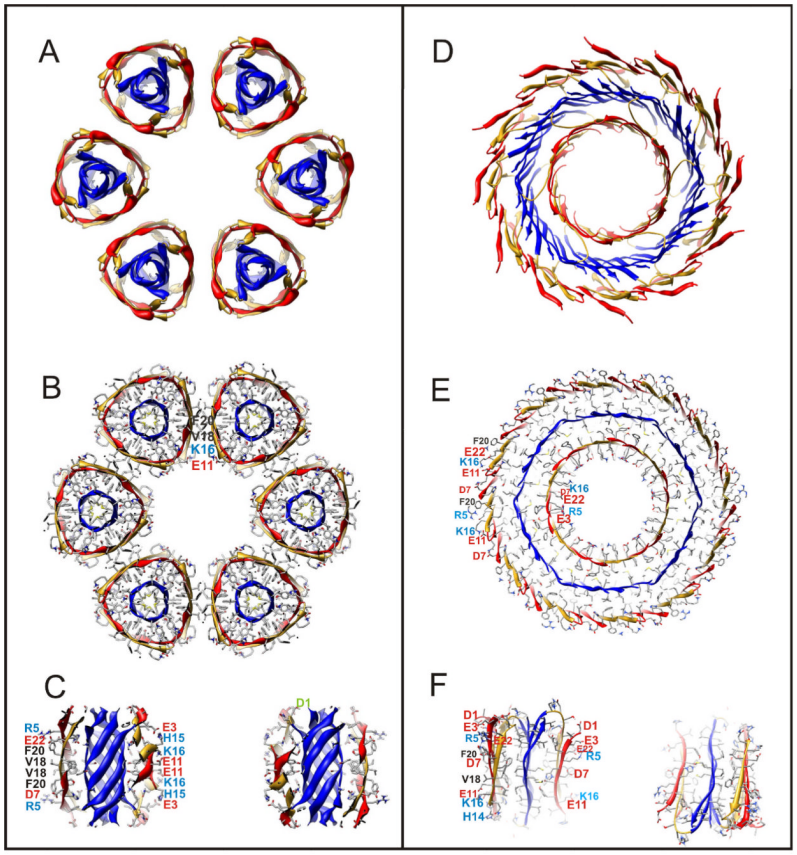

Figure 3.

Models of annular protofibrils formed by 36 Aβ peptides. (A–C) Beaded model formed by six antiparallel ββ-barrel hexamers of the type illustrated in Fig. 1B. (A) Ribbon representation of top view showing the entire assembly. The hexamers are related by 6-fold symmetry about the center of the pore through the protofibril. Adjacent hexamers are related by 2-fold symmetry about an axis parallel to the axes of the barrels and the central 6-fold axis. (B) Cross-section of the central part of the assembly illustrating side chains colored by element. Side chains of the interface between two hexamers are labeled at the top to indicate energetically favorable hydrophobic interactions among V18 and F20 residues of S2 strands at the regions of closest contact between hexamers. (C) Side view of two hexamers on opposite sides of the protofibril. Side chains on the outer layer are labeled and colored blue for positively charged, red for negatively charged, and black for hydrophobic residues. (D–F) Smooth model in which hexamers have merged to form large concentric antiparallel β-barrels; the inner 24-stranded S1–S2 barrel is surrounded by a 36-stranded S3 barrel, which is surrounded by a 48-stranded S1–S2 barrel. D) Ribbon representation of entire assembly. E–F) Cross-sections of central region (E) and side view (F) showing that most side chains buried between barrels are hydrophobic while most side chains exposed on the outer surface or inner pore are hydrophilic. Colored as in Fig. 1. See supplement Movie 1 illustrating the transition from the beaded to smooth model and Fig. Sup9 for results of MD simulations.

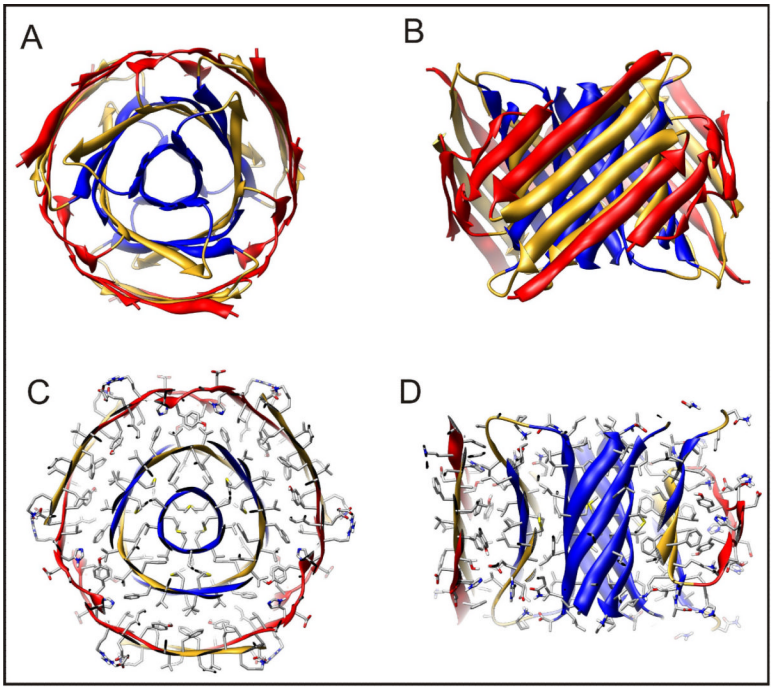

Figure 4.

Models of βββ-barrel dodecamer. (A and B) Ribbon representations view from top (A) down the 3-fold symmetric axis of the barrels and (B) from the side viewed down an axis of 2-fold symmetry. The structure comprises three concentric β-barrels; a central 6-stranded barrel composed of S3 segments of the core subunits, an intermediate 12-stranded barrel composed of S2 segment of the core subunits and S3 segments of the peripheral subunits, and an outer 24 stranded barrel composed of S1 segments of the core subunits and both S1 and S2 segment of the peripheral subunits. (C and D) Cross-sections showing side chains colored by atom type viewed from the top (C) and side (D). Note that for the central region side chains inside the two innermost barrels are all apolar and those between the second and third barrel are either hydrophobic or ambivalent (His or Tyr).

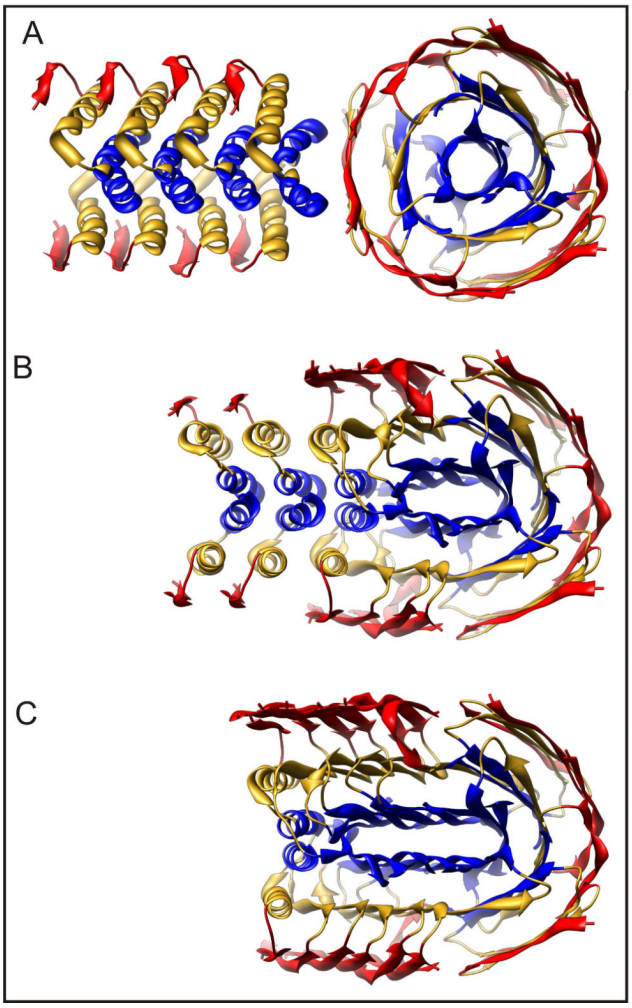

Figure 5.
Models of fibril growth from a dodecamer. (A) A dodecamer model (on right) of the type shown in Fig. 4 is adjacent to a series of four Aβ dimers (on left) that have predominantly helical structures. (B) The β-barrels of the dodecamer have split apart and the most proximal dimer has converted to a predominately β structure and has bound to the edge strands of the dodecamer in a parallel manner. (C) Two more dimers have bound to the growing parallel β sheets formed by S3 (blue), S2 (yellow) and possible S1 (red) segments. The planar sheet portions of these models resemble NMR-based models of Aβ fibrils[22]. Supplement Movie 2 illustrates the proposed transition.